# Metal−Thiolate Clusters in the C-Terminal Domain of Human Neuronal Growth Inhibitory Factor (GIF)†

Daniel W. Hasler, Peter Faller, and Milan Vašák*

*Biochemisches Institut der Universität Zürich, Winterthurerstrasse 190, CH-8057 Zürich, Switzerland*

*Received June 10, 1998; Revised Manuscript Received August 24, 1998*

ABSTRACT: Neuronal growth inhibitory factor (GIF), a metallothionein-like protein (metallothionein-3), impairs the survival and neurite formation of cultured neurons. Native GIF contains 4 Cu(I) and three Zn(II) ions organized in homometallic metal−thiolate clusters. However, the cluster localization is not known. In this study, the metal−thiolate clusters formed with monovalent and divalent metal ions in the C-terminal domain of human GIF [GIF(32−68)] containing 11 cysteines were investigated. The cluster formation was followed by using electronic absorption, circular dichroism (CD), and magnetic circular dichroism (MCD) spectroscopy, and in the case of Cu(I) complexes also by luminescence spectroscopy at 77 K. Spectroscopic studies on the Cu(I)-GIF(32−68) complexes showed the successive formation of two air-sensitive $Cu_4S_{8-9}$- and $Cu_6S_{11}$-clusters. With Zn(II) and Cd(II) ions, a well-defined $M_4S_{11}$-cluster is formed in which each metal ion is tetrahedrally coordinated by cysteine thiolates. In the $^{113}$Cd NMR spectra of $^{113}Cd_4$-GIF(32−68), recorded at 293 and 323 K, all four $^{113}$Cd resonances at 672.8, 620.9, 629.6, and 564.2 ppm were observed only at 323 K. Their detection at elevated temperature indicates a conformational flexibility of this domain. Evidence for the existence of a $Cd_6$-GIF(32−68) complex, contaning two more weakly bound Cd(II) ions, was also obtained. The formation of this complex requires the transformation of some originally terminal thiolates of the $Cd_4S_{11}$-cluster to bridging thiolates, suggesting a more accessible cluster structure. Such properties of $Cd_4$-GIF(32−68) have not been observed with the $Cd_4S_{11}$-cluster in the isolated α-domain (amino acids 31−61) of metallothioneins. The significance of Cu- and Zn-clusters for the structure of native GIF is discussed.

The neuronal growth inhibitory factor (GIF)[1] has been discovered during the studies of Alzheimer's disease (AD). The pathology of AD brains is characterized by a progressive loss of neurons, the accumulation of extracelluar amyloid plaques, and intraneural neurofibrillary tangles (*1*−*4*). It has been hypothesized that the formation of such structures is due to the lack of neurotrophic factors (*5*). To test this hypothesis, the effect of AD brain extract on neonatal cortical neurons in vitro was examined by Uchida and Tomonaga (1989) (*6*). In these cell culture studies, the AD brain extract showed enhanced neurotrophic activity characterized by a marked dendrite sprouting and increased cell survival compared to that of normal human brain. This neuronal plasticity could be linked to the loss of a growth regulatory activity in AD brains. The protein responsible for this effect has been identified as a neuronal growth inhibitory factor (GIF). This protein is abundant in normal human brains but deficient in AD brains (*7*). Subsequent studies have confirmed the growth inhibitory activity of this protein, but its deficiency in AD brains has been put in question (*8*). However, in recent immunohistochemical studies of the brains of patients with Down syndrome, characterized by an AD type of pathology, the loss of GIF in astrocytes around senile plaques has been demonstrated (*9*).

GIF is a low molecular mass (7−8 kDa) cysteine- and metal-rich protein. The amino acid sequence of human GIF (68 amino acids) exhibits about 70% sequence identity with those of mammalian metallothioneins (MT-1 and MT-2 isoforms), including the preserved array of 20 cysteines (*7*). Molecular biological studies revealed that the GIF gene has a similar size and exon/intron organization and is clustered on the same chromosome as the MT-1 and MT-2 isoforms, leading to its classification as MT-3 (*10*, *11*). Similar amino acid sequences to that of human GIF have also been reported for rat, mouse, porcine, equine, bovine, and canine GIF (*10*, *12*−*15*). Compared to the class of mammalian MT-1/MT-2 sequences, the consensus GIF sequence shows the following prominent differences: (i) a conserved insert of a Thr occurring in the P(3)ETC(6) sequence; (ii) two conserved prolines in the C(6)-P-C-P(9) motif; and (iii) an insert of an acidic hexapeptide in the C-terminal region. Moreover, in contrast to the seven Zn usually present in MT-1/MT-2 (*16*), native human GIF contains four Cu and three Zn (*7*). Two independent studies located the N-terminal part of GIF as the biological active part of the protein (*17*, *18*). Thus, the

† This work was supported in part by Swiss National Science Foundation Grant 32-49460.96, Stipendiendfonds der Basler Chemischen Industrie (D.W.H.), and EMDO Stiftung (P.F.).

* To whom correspondence should be addressed at the Biochemisches Institut der Universität Zürich, Winterthurerstrasse 190, CH-8057 Zürich, Switzerland. Telephone: (+41)-1-635 5552. Fax: (+41)-1−635 6805. E-Mail: mvasak@bioc.unizh.ch.

[1] Abbreviations: AD, Alzheimer's disease; GIF, growth inhibitory factor; GIF(32−68), C-terminal part of human GIF (amino acids 32−68); MT, metallothionein; αMT, isolated α-domain of metallothionein (amino acids 31−61); CD, circular dichroism; MCD, magnetic circular dichroism; LMCT, ligand-to-metal charge transfer; EXAFS, extended X-ray absorption fine structure.

10.1021/bi9813734 CCC: $15.00 
Published on Web 10/01/1998

tryptic fragment (amino acids 1−26) of human GIF, containing two Cu and one Zn, has been shown to exhibit a similar biological activity as native Cu,Zn-GIF. The absence of activity when the metal-free, 2-mercaptoethanol-treated peptide was used signifies the importance of metal ions for the correct polypeptide fold (*18*). In other studies, the biological activity was examined for the synthetic N-terminal peptide (amino acids 1−32) and the recombinant C-terminal peptide (amino acids 32−68) of human and mouse GIF which were reconstituted with three and four Zn(II) ions, respectively. In these studies, only the zinc-containing N-terminal peptide exhibited a growth inhibitory activity, which was found similar to that of reconstituted $Zn_7$-GIF. By mutating the conserved C(6)-P-C-P(9) sequence of the N-terminal peptide to C-S-C-A or C-T-C-T, the neurotrophic activity of the zinc-peptide was abolished (*17*). From these studies, it can be concluded that (i) the N-terminal part of GIF is responsible for the growth inhibitory activity, (ii) the two conserved proline residues are essential for the activity, and (iii) bound metal ions are necessary to stabilize the correct protein fold. The importance of native ions in this protein is exemplified by a substantially lower biological activity found for recombinant human GIF expressed in zinc-containing *E. coli* cultures compared to native human GIF containing four Cu and three Zn (*11*).

Despite the high sequence identity between GIF and MTs, their biological properties differ. MT-1 and MT-2 are inducible proteins which are predominantly expressed in parenchymatous tissues such as liver and kidney. They are believed to be involved in the homeostasis of the essential trace metals Zn and Cu, in the heavy-metal detoxification (Cd, Hg), and in the protection against oxidative stress (*19*). In recent in vitro studies, a role for Zn-MT in the control of cellular Zn distribution as a function of the redox state of the cell has been proposed (*20* and references cited therein). In contrast to MT-1/MT-2, human GIF is found predominantly in the brain and exhibits its biological activity in this tissue. Recently, low levels of GIF mRNA have also been found in some other organs (*21*, *22*). In neuronal cell culture studies, only GIF but not MT-1 and MT-2 exhibited a neurotrophic activity (*8*, *17*). The differences in biological properties and primary structure suggest that substantial alterations of the three-dimensional structure of GIF compared to that established for mammalian MT by NMR and X-ray crystallography (*23*−*25*) exist.

A similar metal content to human GIF, i.e., 4−5 Cu and 2−3 Zn, has also been found in GIF isolated from bovine brains with copper being present in the diamagnetic Cu(I) oxidation state. A remarkable property of native Cu,Zn-GIF is its stability to air oxidation (*12*). Further studies, including EXAFS spectroscopy, showed that the 4−5 Cu(I) and 2−3 Zn(II) ions in bovine GIF are organized in homometallic Cu(I)- and Zn(II)-thiolate clusters which are located in two individual protein domains (*26*, *27*). The coordination geometry of the Cu(I) ions was found predominantly trigonal and that of Zn(II) ions tetrahedral (*27*). It should be noted that no homometallic metal distribution has been reported for the GIF(1−26) fragment mentioned above (*18*). However, the lack of two Cys in the GIF(1−26) fragment, compared to the full-length $\beta$-domain GIF(1−32), together with metal rearrangements during the protein digestion and the fragment isolation might be responsible for the metal content of two Cu(I) and one Zn(II) found.

Table 1: Comparison of the Amino Acid Sequences of the N-Terminal Domain of Human MT-2(31−62) (*19*) and Human GIF(32−68) (*7*)

```
                32  |    40    |    50    |    60    | 68
human GIF(32-68)    KSCCSCCPAECEKCAKDCVCKGGEAAEAEAEKCSCCQ
                    ||||||||  | |||  | |||          |||||
human MT-2(31-61)   KSCCSCCPVGCAKCAQGCICKG......ASDKCSCCA
                31  |    40    |    50          |    60
```

The available spectroscopic information on the structural characteristics of GIF reflects the contributions of both clusters present in the native protein. However, the location of the clusters in the protein structure is currently unknown. With the aim of learning more about the cluster structures and their location, we have initiated metal binding studies on the individual GIF domains with the native Zn(II) and Cu(I) ions and with the Cd(II) ions, often used as a spectroscopic probe for the zinc binding sites in metalloproteins. Such studies are fundamental for further use of the recombinant protein. In our previous studies, the metal−thiolate clusters formed with Zn(II), Cd(II), and Cu(I) in the chemically synthesized human GIF(1−32) have been spectroscopically characterized (*28*). The studies showed that with Cu(I) ions two well-defined Cu(I)-clusters, involving all nine cysteine ligands of GIF(1−32), are formed, i.e., the $Cu_4CysS_9$- and the $Cu_6CysS_9$-cluster. Moreover, only the $Cu_4CysS_9$-GIF(1−32)-cluster exhibited a remarkable stability to air oxidation, a property observed also with native Cu,Zn-GIF. With divalent metal ions, a $Me(II)_3S_9$-cluster developed showing spectral features which substantially differ from those reported for the corresponding $Me(II)_3S_9$-cluster in the $\beta$-domain of mammalian MTs (*28*).

The aim of the present work was to explore the cluster forms generated with monovalent and divalent metal ions in the C-terminal part of human GIF [GIF(32−68)]. The importance of this domain is emphasized by its high amino acid sequence homology among all known GIF sequences. Moreover, a conserved Glu-rich hexapeptide insert may provide a number of potential carboxylate ligands. The metal clusters formed in the GIF(32−68) domain with Cu(I), Zn(II), and Cd(II) ions were characterized by using electronic absorption, circular dichroism (CD), magnetic circular dichroism (MCD), and Cu(I) luminescence spectroscopy. In addition, the $^{113}$Cd NMR characterization of the $^{113}$Cd-GIF(32−68) derivative is presented. The results are compared with the corresponding spectroscopic data obtained on native Cu,Zn-GIF and the α-domain of MT.

## MATERIALS AND METHODS

*Preparation of C-Terminal Peptide GIF(32−68) and Its Metal Derivatives. (A) Peptide Synthesis and Purification.* The C-terminal half of human GIF(32−68) (see Table 1) was synthesized on a ABI 433 A peptide synthesizer by standard F-moc chemistry (0.1 mmol peptide scale) using conditions according to the recommendations of the manufacturer. The crude synthesized peptide was dissolved in 0.1% TFA/5% acetonitrile and upon centrifugation passed over a Sephadex G-10 column using the same solvent. The GIF(32−68) was purified on a semipreparative $C_{18}$ reverse phase HPLC column (Brownlee Aquapore ODS300, 20 $\mu$m, 250 × 10 mm) using 0.1% TFA as buffer A and 0.1%TFA/

60% acetonitrile as buffer B. The volume of the collected fractions was reduced by speed-vac drying. The remaining acetonitrile and TFA was removed using a Sephadex G-25 fast desalting column attached to a Pharmacia FPLC system in 10 mM HCl. The yield of the purified peptide was about 7%. Electrospray mass spectrometry (Sciex API III+) of the purified GIF(32−68) from HPLC (diluted 1:1 with 98% methanol, 2% formic acid) yielded a mass of 3809.0 Da, which agreed well with the calculated mass of 3809.4 Da. Beside this main peptide, no other mass peaks have been detected in this mass range. Using quantitative amino acid analysis (HP Aminoquant II), the molar extinction coefficient of the peptide at 220 nm was determined as $\epsilon_{220} = (2.8 \pm 0.2) \times 10^4$ $M^{-1}$ $cm^{-1}$.

*(B) Metal Derivatives of GIF(32−68).* All solutions used in the preparation of the Zn(II)-, Cd(II)- and Cu(I)-GIF(32−68) were rendered oxygen-free by three freeze−pump−thaw cycles on a vacuum line, and all manipulations were carried out in a nitrogen-purged glovebox. Prior to mixing of apo-GIF(32−68) with the required metal ions, the metal concentration of the freshly prepared stock solution was determined by atomic absorption spectrometry (IL Video 12) and that of the peptide via sulfhydryl concentration. In the latter case, the sulfhydryl reaction with 2,2′-dithiopyridine in 0.2 M sodium acetate/1 mM EDTA (pH 4) was followed spectroscopically and the concentration determined using $\epsilon_{343} = 7600$ $M^{-1}$ $cm^{-1}$ (*29*). Based on the protein concentration determined by the absorption at 220 nm, 10.2 ± 1.1 free SH per apo-GIF(32−68) were found (11 cysteines are present). The individual metal derivatives were prepared as follows. An aliquot of the Zn(II) or Cd(II) solution ($Me^{II}Cl_2$ in 0.1 N HCl) containing 10 equiv of the corresponding metal was added to apo-GIF(32−68) in 10 mM HCl followed by pH adjustment to 7.4 with 0.5 M Tris base. Subsequently, an excess of metal ions was removed by using an approximately 1 mL suspension of Chelex 100 (Biorad) followed by filtration of the sample. The NMR samples of $^{113}Cd_4$-GIF(32−68) were prepared in a similar manner. This sample was then rebuffered into 10 mM Tris-HCl, 75 mM NaCl, pH 7.0, and 10% $D_2O$ was added to provide the field-frequency lock. The NMR sample was concentrated to about 2 mM using ultrafiltration, degassed on a vacuum line, and sealed under nitrogen. The $Cd_4$-GIF(32−68) sample for mass analysis was rebuffered using a Pharmacia G-25 fast desalting column (5 mM ammonium acetate, pH 7.0) and before the measurement mixed with an equal amount of 50% methanol/49% $H_2O$/1% formic acid. In the titration of apo-GIF(32−68) with the Cd(II) ions, 1−7 equiv of Cd(II) solution ($CdCl_2$ in 0.1 N HCl) was added to apo-GIF(32−68) in 10 mM HCl followed by pH adjustment to 7.4 with 0.5 M Tris base or by adding the Cd(II) solution to apo-GIF(32−68) previously adjusted to pH 7.4. Copper complexes were prepared by adding the metal as a stable $[Cu^I(CH_3CN)_4]ClO_4$ complex (*30*) in 5 mM HCl/20% acetonitrile to apo-GIF(32−68) in 10 mM HCl/5% acetonitrile. Subsequently, the pH was raised to 7.4 with 0.5 M Tris base.

*Spectroscopic Measurements.* Electronic absorption spectra were recorded on a Varian Cary 3 spectrometer. CD and MCD measurements were carried out on a Jasco J-715 spectroploarimeter equipped with a 1.5 T electromagnet for room-temperature MCD measurements. The latter spectra were obtained using a parallel and an antiparallel direction of the magnetic field resulting in the sum of CD and MCD contributions. Each spectrum represents an average of three scans to improve the signal-to-noise ratio. The spectral parameters employed were 2 nm slit width, 10 nm $min^{-1}$ scan speed, and 8 s response time. The pure CD and MCD spectra were generated by the appropriate subtraction or addition of the spectra obtained at both directions of the magnetic field. The final spectra were smoothed using the FFT algorithm of the Microcal Origin 4.1 software. The protein concentrations for absorption, CD, and MCD measurements were between 8 and 20 $\mu$M, and a 1 cm path length cuvette was used throughout. The CD spectra are expressed as molar ellipticity, $\Theta$, in units of deg $dmol^{-1}$ $cm^2$, and the MCD spectra as $\Theta_M$, in units of deg $dmol^{-1}$ $cm^2$ $T^{-1}$. Luminescence spectra at 77 K were obtained using a SPEX fluorolog spectrofluorometer fitted with a 1934C phoshorimeter accessory using a 45° detection geometry. The samples were filled into 2 mm i.d. quartz tubes and immersed in a cylindric quartz Dewer vessel filled with liquid nitrogen. Luminescence spectra were recorded at 77 K on the microcrystalline frozen sample using a 50 $\mu$s delay and a 0.3 ms acquisition window with excitation at 300 nm. The 133.33 MHz $^{113}$Cd NMR spectra were recorded on a Bruker AMX-600 spectrometer using a inverse-gated broad-band proton decoupling, a 62 500 kHz spectral width, a 0.13 s acquisition time, and a 2 s pulse repetition rate. The spectra were measured both at 298 and at 323 K.

## RESULTS

*Zn(II)-GIF(32−68) Derivative.* By offering an excess of Zn(II) ions to apo-GIF(32−68), followed by a treatment with the metal chelating resin Chelex 100, a stoichiometry of 3.8 Zn(II) ions per GIF(32−68) was obtained. A similar stoichiometry of 4 Zn(II) for this form has also been found by Sewell et al. (*17*). The electronic absorption, CD, and MCD spectra of apo-GIF(32−68) and the $Zn_4$-GIF(32−68) complex at pH 7.4 are shown in Figure 1. The absorption spectrum of apo-GIF(32−68) is characterized by an unresolved tailing starting at about 250 nm and extending to the far-UV region. The chromophores contributing to this absorption profile include the amide transitions and $CysS^-$ transitions. The contribution of the latter transitions is documented by a weak low-energy feature in the corresponding MCD spectrum, due to a partial deprotonation of the 11 cysteines ($pK_a \approx 8.5$). The reconstituted $Zn_4$-GIF(32−68) form exhibits a similar absorption profile, but of increased intensity at the lower energy region. By analogy to the absorption spectra of $Zn_7$-MTs, the metal-induced feature is assigned to CysS−Zn(II) LMCT transitions (*31*). The corresponding CD spectrum of $Zn_4$-GIF(32−68) shows a negative CD feature characterized by a tailing starting at 250 nm, a band at (−)226 nm, and a negative trough at 222 nm. The MCD spectrum of $Zn_4$-GIF(32−68) shows two well-resolved MCD bands at (−)230 nm and (+)212 nm.

*Cd(II)-GIF(32−68) Derivatives.* Cd(II) is often used to probe for the Zn(II) sites in zinc metalloproteins. Due to the increased covalence of the Cd−S bond, the characteristic CysS−Cd(II) LMCT bands in the UV region of Cd-GIF(32−68) are red-shifted compared to those in $Zn_4$-GIF(32−68), allowing their better separation from polypeptide chain transitions. In addition, the $^{113}$Cd(II) derivative of this peptide enables us to study the structure of the metal centers

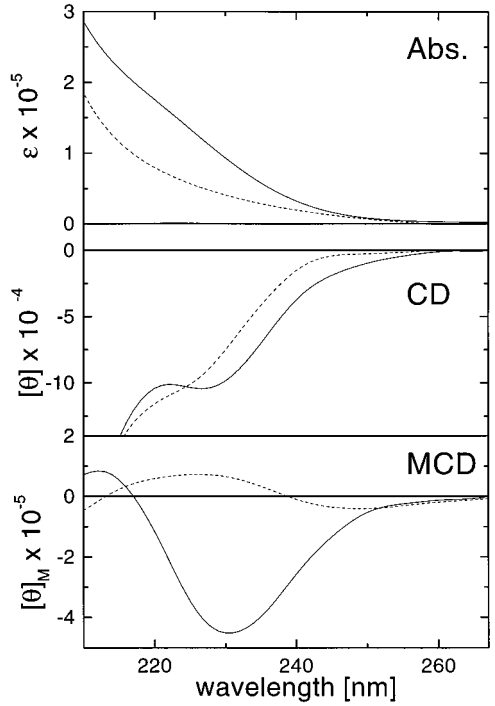


FIGURE 1: Electronic absorption (Abs.), circular dichroism (CD), and magnetic circular dichroism (MCD) spectra of apo-GIF(32−68) (dashed line) and $Zn_4$-GIF(32−68) (solid line) at pH 7.4.

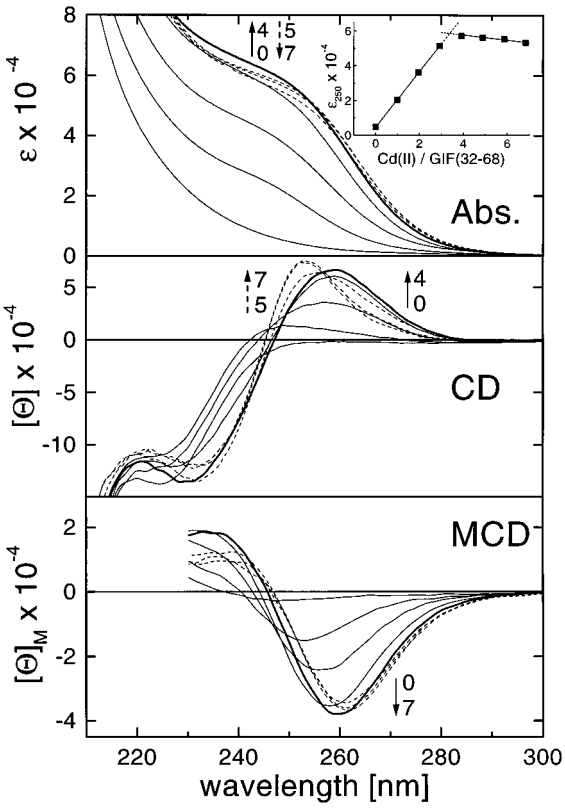


FIGURE 2: Electronic absorption (Abs.), circular dichroism (CD), and magnetic circular dichroism (MCD) spectra of GIF(32−68) recorded as a function of increasing Cd(II) equivalents at pH 7.4. Arrows indicate increasing Cd(II) equivalents present in the individual samples. Solid line: 0, 1.0, 2.0, 2.9. Boldface line: 3.9. Dashed line: 4.9, 5.9, 6.8. Insert: Molar absorption at 250 nm as a function of the mole equivalents of Cd(II) added to apo-GIF-(32−68). For details regarding the sample preparation and the determination of GIF(32−68)-to-metal ratios, see Materials and Methods.

by NMR. In view of a total of seven carboxylate groups in GIF(32−68), which can act as ligands for Cd(II), the binding capacity and spectroscopic properties of Cd-GIF(32−68) were examined using two different approaches. The Cd-GIF(32−68) derivative was prepared in the presence of an excess of Cd(II) ions which were subsequently removed either by exposing to a chelating resin (Chelex 100) or by desalting the sample on a gel filtration column (Pharmacia G-25 fast desalting column) (*32*). However, in both instances, a Cd(II)-to-GIF(32−68) ratio of 4 and closely similar spectroscopic features were obtained. The ES-MS of $^{113}Cd_4$-GIF(32−68) revealed a molecular mass of 4253.0 Da, confirming the binding of four Cd(II) ions (theoretical molecular mass 4253.4 Da). The absorption, CD, and MCD spectra of $Cd_4$-GIF(32−68) are presented in Figure 2 (boldface line). The electronic absorption spectrum of $Cd_4$-GIF(32−68) shows a prominent metal-induced shoulder at about 250 nm, which is typical of the Cd(II)−CysS LMCT transitions (*33*). The molar extinction coefficient of $Cd_4$-GIF(32−68) at 250 nm (58 000 $M^{-1}$ $cm^{-1}$) reveals a value of $5.3 \times 10^3$ $M^{-1}$ $cm^{-1}$ per CysS bound to a Cd(II). This value, which is similar to that reported for a CysS−Cd bond ($\epsilon = 5.5 \times 10^3$ $M^{-1}$ $cm^{-1}$) in a number of Cd-substituted metalloproteins (*34*), strongly suggests that all 11 cysteines of the peptide are involved in metal binding. The corresponding CD spectrum shows a derivative-shaped CD profile with bands at (+)259 and (−)230 nm, and a negative trough around 220 nm. In $Cd_7$-MT, a similar derivative-shaped CD profile has been assigned to an excitonic coupling between transition dipole moments of the bridging thiolate ligands (*35*). By analogy to these studies, the presence of a metal−thiolate cluster in $Cd_4$-GIF(32−68) is inferred. The MCD spectrum of $Cd_4$-GIF(32−68) (Figure 2, boldface line) exhibits MCD bands at (−)260 and (+)238 nm. These features have been assigned to a positive *A*-term originating from a tetrahedrally coordinated metal ion in $Cd_7$-MT (*35*).

To gain insight into the process of cluster formation, a stepwise titration of apo-GIF(32−68) with the Cd(II) ions was also performed. The accompanied spectral changes in the electronic absorption, CD, and MCD spectra as a function of increasing Cd(II) to apo-GIF(32−68) ratios are summarized in Figure 2. In the absorption spectra, the titration of apo-GIF(32−68) with the first 4 Cd(II) equiv is characterized by a progressive red shift of the metal-induced shoulder from 242 to 250 nm. In the case of Cd−thiolate clusters in $Cd_7$-MT, the CysS−Cd(II) LMCT transitions from bridging thiolate ligands are red shifted when compared to those from terminal thiolates (*33*). Thus, the gradual red shift of the absorption envelope of Cd-GIF(32−68) with increasing Cd(II) equivalents suggests that an increasing number of bridging thiolates are involved in metal binding. This is supported by the corresponding MCD spectra where a gradual red shift of both low-energy MCD bands with increasing Cd(II) increments is seen (Figure 2). The observation of only a marginal increase in the absorbance at 250 nm on going from 3 to 4 Cd(II) equiv (Figure 2, insert) indicates that the formation of the final $Cd_4$−thiolate cluster structure involves mainly a transformation of originally terminal thiolate ligands to bridging thiolates and must, therefore, be accompanied by major structural changes. This inference is supported by the corresponding CD spectra

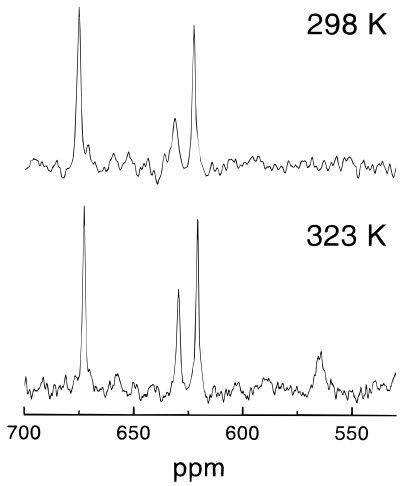


FIGURE 3: 133.33 MHz $^{113}Cd$ NMR spectra of $^{113}Cd_4$-GIF(32−68) at 298 K (top) and 323 K (bottom). Conditions: 2 mM protein sample in 10 mM Tris-HCl, 75 mM NaCl at pH 7.0.

where the excitonic CD bands develop with the last Cd(II) equivalent added. From these studies, it can be concluded that the $Cd_4$−thiolate cluster in $Cd_4$-GIF(32−68) is formed in a noncooperative fashion.

As shown above, the isolated $Cd_4$-GIF(32−68) form represents the fully metal loaded peptide. However, from the titration studies, evidence for additional metal binding sites exists (Figure 2). This is documented by spectral changes of the $Cd_4$-GIF(32−68) profile with an additional 2 Cd(II) equiv. Thus, while only minor spectroscopic changes are seen in the absorption and MCD spectra, a pronounced effect is discerned in the corresponding CD spectra. These CD changes can be interpreted in terms of additional metal binding which alters the structure of the $Cd_4$-cluster. It can be concluded, therefore, that the binding of Cd(II) to GIF(32−68) generates, besides the stable $Cd_4$-cluster form, a $Cd(II)_6$ complex with an additional two weakly bound Cd(II) ions. As the MCD band is further red shifted, additional terminal cysteines have to be transformed to bridging ones.

*$^{113}Cd$ NMR Studies of $^{113}Cd_4$-GIF(32−68).* $^{113}Cd$ NMR spectroscopy has been widely used in studies on the metal binding sites in MTs. The one-dimensional $^{113}Cd$ NMR spectra of mammalian $Cd_7$-MTs usually exhibit seven $^{113}Cd$ resonances corresponding to the seven metals bound. The $^{113}Cd$ resonances are typically found between 600 and 700 ppm relative to the external standard $^{113}Cd(ClO_4)_2$. The $^{113}Cd$ NMR spectra of $^{113}Cd_4$-GIF(32−68) were recorded at 298 and 323 K (Figure 3). The spectrum recorded at 298 K shows three $^{113}Cd$ resonances for four metal ions, i.e., two major $^{113}Cd$ resonances of about the same intensity at 622.8 and 675.4 ppm and a smaller, rather broad resonance at 631.3 ppm. The observed features suggest the presence of dynamic processes precluding the detection of all resonances. This is confirmed by the $^{113}Cd$ NMR spectrum recorded at higher temperature. At 323 K, four $^{113}Cd$ resonances were detected: two strong resonances at 672.8 and 620.9 ppm, a resonance of medium intensity at 629.6 ppm, and a small, broad resonance at 564.2 ppm. The appearance of the 564.2 ppm signal at higher temperature can be accounted for by a change in the time scale from an intermediate to a fast exchange process (Table 2).

Table 2: Chemical Shift Positions of $^{113}Cd$ Resonances in Human $^{113}Cd_7$-MT-2 (*24*), Human $^{113}Cd_4$-MT-2 α-Domain (*42*), and Human $^{113}Cd_4$-Gif(32−68)

| | chemical shift (ppm) | | | | temp (K) |
|---|---|---|---|---|---|
| $Cd_4$-GIF(32−68), 298 K | 675.8 | 631.3 | 622.8 | | 298 |
| $Cd_4$-GIF(32−68), 323 K | 672.8 | 629.6 | 620.9 | 564.2 | 323 |
| $Cd_4$-MT-2 α-domain (αMT2) | 669 | 630 | 627 | 605 | 295 |
| $Cd_4$-cluster in $Cd_7$-MT-2 | 674 | 634 | 629 | 617 | 298 |
| $Cd_3$-cluster in $Cd_7$-MT-2 | 672 | 652 | 650 | | 298 |

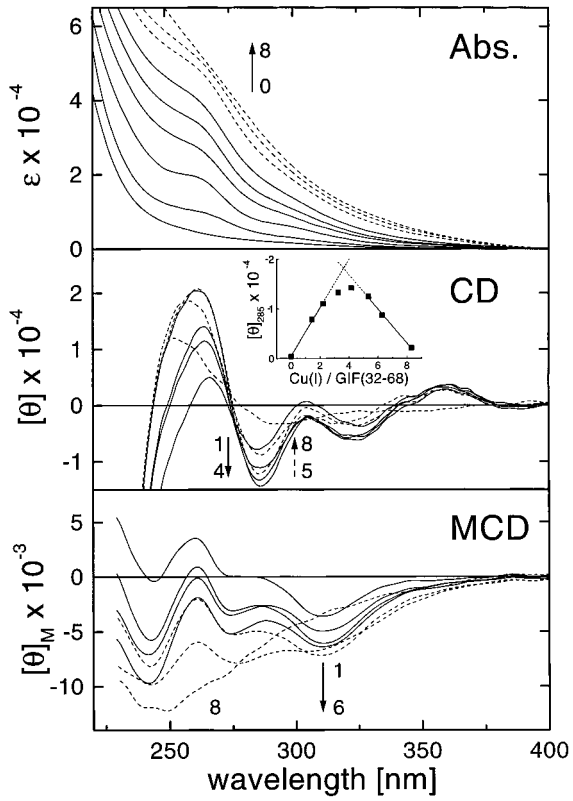


FIGURE 4: Electronic absorption (Abs.), circular dichroism (CD), and magnetic circular dichroism (MCD) spectra of GIF(32−68) recorded as a function of increasing Cu(I) equivalents at pH 7.4. Arrows indicate increasing Cu(I) equivalents present in the individual samples. Solid line: 1.4, 2.2, 3.3, 4.2. Dashed line: 5.4, 6.3, 8.2. Insert: Molar ellipticity at 285 nm as a function of the mole equivalents of Cu(I) added to apo-GIF(32−68). For details regarding the sample preparation and the determination of GIF-(32−68)-to-metal ratios, see Materials and Methods.

*Cu(I)-GIF(32−68) Derivatives.* To examine the binding capacity of GIF(32−68) with Cu(I) ions, the complexes formed with increasing mole equivalents of copper were spectroscopically characterized. The electronic absorption, CD, and MCD spectra are presented in Figure 4. The broad electronic absorption spectra of Cu-GIF(32−68) complexes are characterized by a pronounced shoulder at about 260 nm, a weaker shoulder at about 300 nm, and a tailing to 375 nm. These spectral features increase in intensity with the first about 6 Cu(I) equiv. Further addition of about 2 Cu(I) equiv is accompanied only by a minor alteration of the spectral profile. Closer examination of the development of these spectral features reveals that the intensity of the shoulder at 260 nm is increasing more or less linearly up to about 5 Cu(I) equiv followed mainly by a red shift of the absorption profile when a further 3 Cu(I) equiv is added. The corresponding CD spectra show a number of well-resolved

CD bands at (+)358, (−)323, (+)305, (−)285, and (+)260 nm. The two low energy CD bands developing with the first about 2 Cu(I) equiv remain unchanged with an additional 2 Cu(I) equiv added and slowly disappear with the last about 4 Cu(I) equiv. In contrast, the high-energy CD bands at (+)-305 and (−)285 nm reach a maximum intensity with the first about 4 Cu(I) equiv. The plot of the intensity of the (−)285 nm band as a function of Cu(I) equivalents bound clearly demonstrates the formation of a distinct $Cu_4$-GIF-(32−68) complex (Figure 4, insert). However, in the corresponding MCD spectra, a broad negative MCD band at about 310 nm shows a maximum intensity between 5 and 6 Cu(I) equiv bound. This and the presence of only minor changes in the absorption profile on going from 6 to 8 Cu-(I) equiv indicate that full peptide saturation with 6 Cu(I) equiv occurred, i.e., a $Cu_6$-GIF(32−68) complex. Thus, it appears that with Cu(I) ions two complexes are formed, $Cu_4$-GIF(32−68) and $Cu_6$-GIF(32−68).

Further structural information about the Cu(I)-GIF(32−68) complexes relies on the knowledge of the spectral origin of the absorption, CD, and MCD bands. The spectroscopic features of the Cu-GIF(32−68) complexes can be separated into two spectral regions, the low-energy region (above 300 nm) with electronic transitions of only small extinction coefficients but relatively strong CD and MCD features and the high energy region where large extinction coefficients occur. The presence of intense CD and MCD bands at wavelengths where rather low extinctions occur is typical for electric dipole forbidden but magnetic dipole allowed transitions. In Cu(I)−MT complexes, this feature has been assigned to formally spin-forbidden 3d → 4s metal cluster-centered transitions brought about by Cu(I)−Cu(I) interactions in polynuclear Cu(I) complexes (*36* and references cited therein). Therefore, the presence of similar low-energy features in the $Cu_4$- and $Cu_6$-GIF(32−68) complexes indicates the existence of Cu(I)-polyhedra. The bands in the high-energy region (below 280 nm) originate predominantly from CysS−Cu(I) LMCT transitions (*36*). It has been shown, moreover, that the intensity of the 262 nm LMCT transition reflects the number of thiolate ligands involved in metal binding with an extinction coefficient of about 5200−5500 $M^{-1}$ $cm^{-1}$ per Cu(I)−S bond. Using this value and the molar absorption of the $Cu_4$-GIF(32−68) complex ($\epsilon_{262\ nm} \approx 41\ 000\ M^{-1}\ cm^{-1}$) suggest that only about 8−9 of the 11 cysteines are involved in the metal binding. Conversely, in the $Cu_6$-GIF(32−68) complex ($\epsilon_{262} \approx 55\ 000\ M^{-1}\ cm^{-1}$), all 11 cysteines would participate in metal coordination. This finding is supported by the accessibility of these free cysteine thiolates to modification with 2,2′-dithiopyridine in the case of $Cu_4$-GIF(32−68) but not in $Cu_6$-GIF(32−68).

*Luminescence Spectra of Cu-GIF(32−68) Forms.* Another widely used technique for studying Cu(I) complexes is luminescence spectroscopy. The low-temperature luminescence (77 K) has been used to study inorganic Cu(I)-clusters (*37*) and Cu(I)-MTs (*36*). The luminescence spectra developing upon the binding of Cu(I) ions to MT are characterized by two emissive bands centered at 420 and 600 nm showing lifetimes of about 50 and 130 ms, respectively. Both the lifetimes of the emission and the large Stoke's shift are consistent with their originating from triplet excited states. These emissions have been attributed to arise from two distinct triplet excited-state manifolds which are

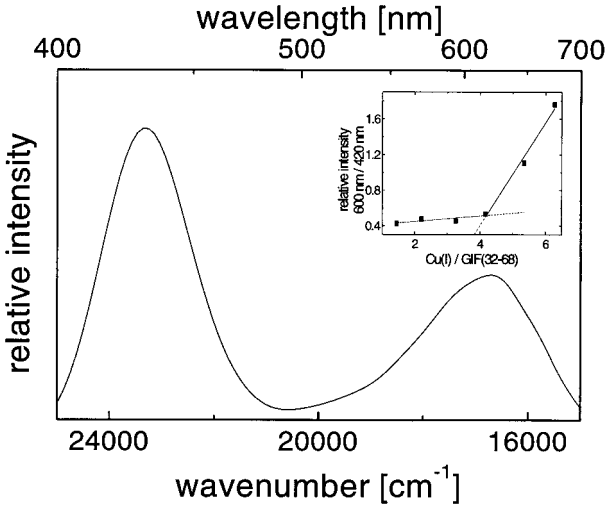


FIGURE 5: Representative luminescence spectrum of $Cu_4$-GIF(32−68) at 77 K. Insert: Dependence of the Cu(I)/apo-GIF(32−68) ratio on the relative emission ratio 600/420 nm.

mixed LMCT/d−s transitions in origin (*36*, *37*). The 420 nm emissive band has been attributed to a predominantly cluster-centered transition in origin, being delocalized over the metal core, whereas the 600 nm emissive band has been assigned to a transition which is mainly composed of ligand p orbitals. The representative luminescence spectrum developing upon the binding of four Cu(I) ions to GIF(32−68) is illustrated in Figure 5. The spectroscopic characteristics of the $Cu_4$-GIF(33−68) form were found closely similar to those reported for Cu(I)-MT (*36*). The intensity ratio between the emissive bands at 420 and 600 nm remains constant between 1 and 4 Cu(I) equiv bound to apo-GIF-(32−68) (Figure 5, insert). However, when more than 4 Cu(I) equiv is bound, the band at 420 nm became substantially less intense compared to that at 600 nm. This behavior, which manifests itself by the presence of a breaking point at the Cu(I)-to-apo-GIF(32−68) ratio of 4 (Figure 5, insert), is in agreement with the formation of a $Cu_4$-$CysS_{8-9}$ cluster undergoing structural changes with additional Cu(I) equivalents.

*Stability of Cu-GIF(32−68) Forms in Air*. The instability of mammalian Cu(I)-MTs in air is well documented (*38*). A striking feature of native Cu,Zn-GIF is its stability to air oxidation (*26*). In studies of GIF(1−32), containing nine cysteines, the formation of $Cu_4S_9$- and $Cu_6S_9$-clusters has been shown. However, only the $Cu_4S_9$-cluster showed a remarkable stability to air oxidation (*28*). This behavior is quite unusual for Cu(I)−thiolate clusters. Therefore, the stability in air of both Cu(I)-clusters formed with apo-GIF-(32−68) was also examined. Upon exposure of nitrogen-saturated $Cu_4$-GIF(32−68) solution to air, a marked intensity decrease of the absorption band at 260 nm over a time period of 3 h occurred. Similar studies using the $Cu_6$-GIF(32−68) form revealed slower, but still pronounced gradual spectral changes of both shape and intensity of the absorption profile during the same time period (data not shown). Thus, both $Cu_4$- and $Cu_6$-GIF(32−68) clusters are prone to air oxidation.

## DISCUSSION

As discussed above, the bound metal ions are crucial for the development of the biologically active structure of GIF.

In biological assays, both native human Cu,Zn-GIF and the Zn-reconstituted recombinant human $Zn_7$-GIF were found biologically active. However, the biological activity of recombinant GIF expressed in Zn-containing *E. coli* cultures was found substantially lower when compared with that of native Cu,Zn-GIF (*11*). In other studies, the reconstituted Cu,Zn-GIF form, generated by the addition of 6 Cu(I) equiv to recombinant $Zn_7$-GIF, was found neurotoxic (*17*). To reinvestigate the biological effect of Cu(I) ions in the protein, we have examined the biological activity of native bovine Cu,Zn-GIF using a new neuronal assay. In this assay, similar to human Cu,Zn-GIF, no neurotoxic effect was found. Moreover, native bovine Cu,Zn-GIF affected neuronal cell cultures in a tissue-specific manner (*39*). Thus, knowledge about the metal−thiolate clusters in GIF is of great importance for further studies of this protein.

The results of these studies demonstrate that the binding of Zn(II) and Cd(II) ions to apo-GIF(32−68) generates a metal−thiolate cluster structure, $Me^{II}_4CysS_{11}$. In the α-domain of all structurally characterized vertebrate MT-1/MT-2, a well-defined $Me(II)_4CysS_{11}$ cluster exists (*16*, *35*, *40*). The presence of an MT-type $Me(II)_3CysS_9$ cluster also in GIF(1−32) (*28*) strongly suggests that in GIF a similar two-domain structure as found for mammalian $Me(II)_7$-MT exists. However, although the metal-to-cysteine stoichiometries in both GIF domains are identical to those established for MT, their spectral properties substantially differ. Thus, based on the widely different spectroscopic features of the $Me(II)_3$-GIF(1−32) cluster, it has been concluded that the structural changes introduced by the conserved C(6)-P-C-P(9) sequence are more profound and not restricted to a local alteration of the domain structure (*28*). A similar conclusion can be drawn from the present studies of GIF(32−68). In contrast to the isolated α-domain of rat liver MT-2 (αMT-2) (*41*) and human liver αMT-2 (*42*), in GIF(32−68) the $Cd_4CysS_{11}$-cluster is formed in a noncooperative fashion. Moreover, no additional metal binding has been found in the former studies. In GIF(32−68), the binding of an additional 2 Cd(II) ions to $Cd_4$-GIF(32−68) generates the $Cd_6$-GIF(32−68) form. The accompanied red shift in the absorption and MCD spectra indicates the transformation of some terminal thiolates to bridging thiolate ligands (*33*), an effect consistent with an increased accessibility of the $Cd_4$-cluster. In this case, besides cysteine sulfurs additional Cd(II) coordinating ligands provided by the peptide, e.g., oxygen, or solvent are also likely.

The major difference between the primary structures of GIF(32−68) and the α-domain of MT is the presence of an acidic hexapeptide insert, G(54)EAAEA(59). This peptide insert is linked to the additional acidic tripeptide E(60)AE-(62), which also differs from the corresponding vertebrate MT consensus sequence A(53)SD(55) (see Table 1). These amino acid residues in GIF together with the 2 residues, K(52)G(53), present in both GIF and MT generate a 12 amino acid loop connecting the flanking cysteine ligands, i.e., Cys(51) and Cys(64). We infer that the electrostatic repulsion between this acidic loop and the negatively charged $Me(II)_4CysS_{11}$-cluster leads to a more open structure resulting in an increased accessibility of the metal-cluster to solvent and ions. This conclusion is in agreement with the additional Cd(II) binding to the $Cd_4$-$CysS_{11}$-cluster of GIF(33−68). Moreover, it would be expected that such a less constrained structure of $Cd_4$-GIF(32−68) would facilitate exchange processes. Indeed, in the $^{113}$Cd NMR spectra of this domain, dynamic processes were observed. This is exemplified by temperature-dependent changes of $^{113}Cd_4$-GIF(32−68) on going from 297 to 323 K, where, besides substantial sharpening of the three $^{113}$Cd resonances at 672.8, 629.6, and 620.9 ppm, a new, originally unobserved broad resonance at 564.2 ppm occurred. The resonances at 672.8, 629.6, and 620.9 ppm occur at a similar position reported for the $^{113}Cd_4$-cluster in the isolated human αMT-2 domain at 295 K. In this case, $^{113}$Cd resonances at 669, 630, and 627 ppm, and a broad resonance at 605 ppm, were detected (Table 2) (*42*). However, in the latter studies, no evidence for dynamic processes was obtained. It may be noted that a close correspondence between the chemical shift positions of the $^{113}$Cd resonances in both the individual $^{113}Cd_4$-αMT-2 and $^{113}Cd_7$-MT-2 exists, the only exception being a downfield shift of the 605 ppm resonance in $^{113}Cd_4$-α-MT-2 to 617 ppm in $^{113}Cd_7$-MT-2 (*24*). Consequently, the chemical shift position of the 564.2 ppm resonance of $^{113}Cd_4$-GIF(32−68) lies out of the range of the metal sites coordinated by terminal and bridging thiolates found in MTs. However, as at 323 K the 564.2 ppm resonance is under fast chemical exchange, the exact chemical shifts of the corresponding states are unknown. Nevertheless, the NMR properties of this site are consistent with altered metal coordination(s). Currently, we ascribe this effect to a perturbation of the thiolate coordination sphere by some exogenous or endogenous ligands.

In the high-energy region of the CD spectrum of $Cd_4$-GIF(32−68), a negative trough at about 220 nm is discerned (Figure 2). In contrast, this CD feature in the isolated $Cd_4$-αMT-2 is present as a pronounced positive CD band at 223 nm (*41*). The secondary structure prediction program SSCP of Eisenhaber et al. (*43*, *44*) applied to this peptide loop (amino acids 52−63) revealed about 85% α-helical structure with both algorithms of this program. Thus, in $Cd_4$-GIF-(32−68), a spectral compensation of this positive CD band by negative CD features of an α-helical structure occurring at 222 nm would be conceivable.

With Cu(I) ions, two well-defined Cu(I)−thiolate clusters in the GIF(32−68) domain are formed, i.e., the $Cu_4CysS_{8-9}$- and $Cu_6CysS_{11}$-clusters. The simplest crystallographically defined inorganic model possessing a polynuclear $Cu_4S_9$ core is that of the Cu(I)−thiourea complex, i.e., $Cu_4[SC(NH_2)_2]_9^{4+}$. This structure is adamantane-like with one trigonal planar copper and three very distorted tetrahedral copper species (*45*). The formation of a $Cu_6S_{11}$-cluster has also been reported for the individual αMT-2 domain. For this $Cu_6S_{11}$-cluster, a digonal and trigonal Cu(I) coordination has been proposed (*38*, *46*−*48*). In native Cu,Zn-GIF, the low-energy features (above 240 nm) in the absorption, CD, and MCD spectra, originating from a Cu(I)−thiolate cluster, are well separated from those of the Zn(II)−thiolate cluster occurring at higher energy (*26*). This allows their comparison with both Cu(I)-GIF(32−68) complexes. A close correspondence is discerned between the CD and MCD features of native Cu,Zn-GIF and those presented in this study for the $Cu_4$-$CysS_{8-9}$-cluster. However, these spectral features in native Cu,Zn-GIF are more intense (about 30%) and less well resolved. Moreover, in contrast to native Cu,Zn-GIF and $Cu_4$-GIF(1−32), both $Cu_4$- and $Cu_6$-clusters in GIF(32−68) are susceptible to air oxidation. It seems, therefore, unlikely

that a $Cu(I)_4$-$CysS_{8-9}$ cluster would be located in the α-domain of native Cu,Zn-GIF. At present, the spectroscopic features of Cu(I) complexes in both GIF domains do not allow an unambiguous assignment to the location of the Cu-cluster in native Cu,Zn-GIF. However, in view of the $^{113}Cd$ NMR characterization of $Cd_4$-GIF(32−68), the $^{113}Cd$ NMR study of GIF containing both the Cu(I) and $^{113}Cd$(II) ions should yield this information. This knowledge is of great importance for future use of recombinant protein since from *E. coli* cultures a metalloform containing both metal ions cannot be isolated.

In conclusion, besides the formation of distinct metal−thiolate clusters, the other major finding of these studies is the enhanced flexibility of the $Cd_4$-GIF(32−68) domain. Even larger flexibility has been found with the $Zn_3$- and $Cd_3$-GIF(1−32) domains (*28*). These properties of GIF structure may be important for the biological function of this protein, playing a role in protein−protein or protein−receptor interaction.

## ACKNOWLEDGMENT

The expert assistance of Dr. S. Klauser with the synthesis of the peptide and Dr. P. Gehrig in obtaining the ESI-MS spectra is gratefully acknowledged. We also thank N. Walch and M. Binder for recording the NMR spectra.

## REFERENCES

1. Selkoe, D. J. (1991) *Neuron 6*, 487−498.
2. Sisodia, S. S., and Price, D. L. (1995) *FASEB J. 9*, 366−370.
3. Goedert, M. (1993) *Trends Neurosci. 16*, 460−465.
4. Edelberg, H. K., and Wei, J. Y. (1996) *Mech. Ageing Dev. 91*, 95−114.
5. Appel, S. H. (1981) *Ann. Neurol. 10*, 499−505.
6. Uchida, Y., and Tomonaga, M. (1989) *Brain Res. 481*, 190−193.
7. Uchida, Y., Takio, K., Titani, K., Ihara, Y., and Tomonaga, M. (1991) *Neuron 7*, 337−347.
8. Erickson, J. C., Sewell, A. K., Jensen, L. T., Winge, D. R., and Palmiter, R. D. (1994) *Brain Res. 649*, 297−304.
9. Arai, Y., Uchida, Y., and Takashima, S. (1997) *Pediatr. Neurol. 17*, 134−138.
10. Palmiter, R. D., Findley, S. D., Whitmore, T. E., and Durnam, D. M. (1992) *Proc. Natl. Acad. Sci. U.S.A. 89*, 6333−6337.
11. Tsuji, S., Kobayashi, H., Uchida, Y., Ihara, Y., and Miyatake, T. (1992) *EMBO J. 11*, 4843−4850.
12. Pountney, D. L., Fundel, S. M., Faller, P., Birchler, N. E., Hunziker, P., and Vašák, M. (1994) *FEBS Lett. 345*, 193−197.
13. Kobayashi, H., Uchida, Y., Ihara, Y., Nakajima, K., Kohsaka, S., Miyatake, T., and Tsuji S. (1993) *Mol. Brain Res. 19*, 188−194.
14. Chen, C. F., Wang, S. H., and Lin, L. Y. (1996) *Comp. Biochem. Physiol. 115B*, 27−32.
15. Kojima, S., Shimada, A., Kodan, A., Kobayashi, K., Morita, T., Yamano, Y., and Umemura, T. (1998) *Can. J. Vet. Res. 62*, 148−151.
16. Vašák, M., and Kägi, J. H. R. (1994) in *Encyclopedia of Inorganic Chemistry, Volume 4* (King, R. B., Ed.) pp 2229−2241, J. Wiley & Sons Ltd., New York.
17. Sewell, A. K., Jensen, L. T., Erikson, J. C., Palmiter, R. D., and Winge, D. R. (1995) *Biochemistry 34*, 4740−4747.
18. Uchida, Y., and Ihara, Y. (1995) *J. Biol. Chem. 270*, 3365−3369.
19. Kägi, J. H. R. (1993) in *Metallothioneins III* (Suzuki, K. T., Imura, N., and Kimura, M., Eds.) pp 29−56, Birkhäuserverlag, Basel.
20. Maret, W., and Vallee, B. L. (1998) *Proc. Natl. Acad. Sci. U.S.A. 95*, 3478−3482.
21. Hoey, J. G., Garrett, S. H., Sens, M. A., Todd, J. H., and Sens, D. A. (1997) *Toxicol. Lett. 92*, 149−160.
22. Moffatt, P., and Séguin, C. (1998) *DNA Cell Biol. 6*, 501−510.
23. Messerle, B. A., Schäffer, A., Vašák, M., Kägi, J. H. R., and Wüthrich, K. (1990) *J. Mol. Biol. 214*, 765−779.
24. Braun, W., Vašák, M., Robbins, A. H., Stout, C. D., Wagner, G., Kägi, J. H. R., and Wüthrich, K. (1992) *Proc. Natl. Acad. Sci. U.S.A. 89*, 10124−10128.
25. Robbins, A. H., McRee, D. E., Williamson, M., Collett, S. A., Xuong, N. H., Furey, W. F., Wang, B. C., and Stout, C. D (1991) *J. Mol. Biol. 221*, 1269−1293.
26. Bogumil, R., Faller, P., Pountney, D. L., and Vašák, M. (1996) *Eur. J. Biochem. 238*, 698−705.
27. Bogumil, R., Faller, P., Binz, P.-A., Vašák, M., Charnock, J. M., and Garner, C. D. (1998) *Eur. J. Biochem. 255*, 172−177.
28. Faller, P., and Vašák, M. (1997) *Biochemistry 36*, 13341−13348.
29. Pedersen, A. O., and Jacobsen, J. (1980) *Eur. J. Biochem. 106*, 291−295.
30. Hemmerich, P., and Sigwart, C. (1963) *Experientia 19*, 488−489.
31. Vašák, M., Kägi, J. H. R., and Hill, H. O. A. (1981) *Biochemistry 20*, 2852−2856.
32. Vašák, M. (1991) *Methods Enzymol. 205*, 452−458.
33. Willner, H., Vašák, M., and Kägi, J. H. R. (1987) *Biochemistry 26*, 6287−6292.
34. Henehan, C. J., Pountney, D. L., Zerbe, O., and Vašák, M. (1993) *Protein Sci. 2*, 1756−1764.
35. Stillmann, M. J. (1992) in *Metallothioneins* (Stillman, M. J., Shaw, C. F., III, and Suzuki, K. T., Eds.) pp 55−127, VCH, New York.
36. Pountney, D. L., Schauwecker, I., Zarn, J., and Vašák, M. (1994) *Biochemistry 33*, 9699−9705.
37. Ford, P. C., and Vogler, A. (1993) *Acc. Chem. Res. 26*, 220−226.
38. Winge, D. R. (1991) *Methods Enzymol. 205*, 458−469.
39. Bruinink, A., Faller, P., Sidler, C., Bogumil, R., and Vašák, (1998) *Chem. Biol. Interact.* (in press).
40. Vašák, M., and Kägi, J. H. R. (1983) *Met. Ions Biol. Syst. 15*, 213−275.
41. Stillmann, M. J., Cai, W., and Zelazowski, A. J. (1987) *J. Biol. Chem. 262*, 4538−4548.
42. Kull, F. J., Reed, M. F., Elgren, T. E., Ciardelli, T. L., and Wilcox, D. E. (1990) *J. Am. Chem. Soc. 112*, 2291−2298.
43. Eisenhaber, F., Imperiale, F., Argos, P., and Frömmel, C. (1996) *Proteins: Struct., Funct., Genet. 25*, 157−168.
44. Eisenhaber, F., Frömmel, C., and Argos, P. (1996) *Proteins: Struct., Funct., Genet. 25*, 169−179. See as well: Eisenhaber, F., and Imperiale F. (1995) Program SSCP, version 1.1 (September 1995), http://www.embl-heidelberg.de/argos/ASC.21/eisenhaber-home.html.
45. Griffith, E. H., Hunt, G. W., and Amma, E. L. (1976) *J. Chem. Soc., Chem. Commun*. 432−433.
46. Chen, P., Munoz, A., Nettesheim, D., Shaw, C. F., III, and Petering, D. H. (1996) *Biochem. J. 317*, 395−402.
47. Li, Y. J., Zhang, L. S., Bayer, E., Oelkrug, D., and Weser, U. (1990) *Z. Naturforsch. 45C*, 1193−1196.
48. Li, Y.-J., and Weser, U. (1992) *Inorg. Chem. 31*, 5526−5533.

BI9813734